HAL
open science

Spark plasma sintering of Sb2Se3 sputtering target towards highly efficient thin film solar cells

G. Liang, X. Chen, R. Tang, Y. Liu, Y. Li, P. Luo, Z. Su, Xianghua Zhang, P. Fan, S. Chen

To cite this version:

G. Liang, X. Chen, R. Tang, Y. Liu, Y. Li, et al.. Spark plasma sintering of Sb2Se3 sputtering target towards highly efficient thin film solar cells. Solar Energy Materials and Solar Cells, 2020, 211, pp.110530. 10.1016/j.solmat.2020.110530 . hal-02536599

HAL Id: hal-02536599

https://univ-rennes.hal.science/hal-02536599v1

Submitted on 15 Jun 2023

HAL is a multi-disciplinary open access archive for the deposit and dissemination of scientific research documents, whether they are published or not. The documents may come from teaching and research institutions in France or abroad, or from public or private research centers.

L'archive ouverte pluridisciplinaire **HAL**, est destinée au dépôt et à la diffusion de documents scientifiques de niveau recherche, publiés ou non, émanant des établissements d'enseignement et de recherche français ou étrangers, des laboratoires publics ou privés.

Spark plasma sintering of Sb_2Se_3 sputtering target towards highly efficient thin film solar cells

Guangxing Liang,[a] Xingye Chen,[a] Rong Tang,[a] Yike Liu,[b] Yingfen Li,[b] Ping Luo,[a] Zhenghua Su,[a] Xianghua Zhang,[c] Ping Fan,[a] Shuo Chen[a,*]

[a]*Shenzhen Key Laboratory of Advanced Thin Films and Applications, College of Physics and Optoelectronic Engineering, Shenzhen University, Shenzhen, 518060, China*

[b]*School of Material and Metallurgical Engineering, Guizhou Institute of Technology, Guiyang 550003, China*

[c]*Univ Rennes, CNRS, ISCR (Institut des Sciences Chimiques de Rennes) UMR 6226, F-35000 Rennes, France*

[*]Corresponding author: Email: chensh@szu.edu.cn (Prof. Chen)

ABSTRACT: Antimony selenide (Sb_2Se_3) is a potential absorber material for environment-friendly and cost-efficiently photovoltaics due to its material advantages and superior optoelectronic properties. In this work, we proposed a facile and versatile method of ball milling followed with spark plasma sintering (SPS) to prepare high-quality Sb_2Se_3 sputtering target. Then the highly crystalline Sb_2Se_3 thin film consisted of large crystal grains can be prepared by using radio frequency (RF) magnetron sputtering with an additional post-selenization heat treatment. An efficient substrate structured Sb_2Se_3 thin film solar cell with configuration of Mo/Sb_2Se_3/CdS/ITO/Ag was fabricated and a champion device with highly interesting power conversion efficiency (PCE) of 5.08% has been achieved. Superior device performances are closely related to the Sb_2Se_3 absorber layer with benign growth orientation and the Sb_2Se_3/CdS heterojunction interface with smooth contact,

which induced less recombination loss. The combined features of homemade sputtering target and advantageous thin film preparation technology further demonstrated its attractive application potential in thin film photovoltaic scenarios.

KEYWORDS: Sb_2Se_3, sputtering target, spark plasma sintering, magnetron sputtering, post-selenization, thin film solar cells

1. Introduction

Solar cells which can directly convert solar energy into electric power have drawn tremendous research attentions because of the potential to partially compensate the non-renewable fossil fuels.[1-3] Among various kinds of solar cells, silicon-based series, copper indium gallium selenide (CIGS) and cadmium telluride (CdTe) thin films are the dominant materials currently used in photovoltaic scenarios and all of them have achieved certified power conversion efficiency (PCE) higher than 20%.[4-7] However, the intrinsic indirect band gap and a relatively low absorption coefficient of Si requires a thick wafer to absorb sunlight, which still costs more than traditional fuels in power production.[4] The natural scarcity of Te, In and Ga on Earth, as well as the toxicity of Cd are the main concerns for CIGS and CdTe solar cells.[8] Thus, alternative environment-friendly and cost-efficiently photovoltaic materials are urgently required and actively investigated. The binary semiconductor of antimony selenide (Sb_2Se_3) can be considered as a promising candidate because of its attractive optoelectronic properties, such as an appropriate band gap (1.1-1.3 eV, approaching the ideal Shockey-Queisser value), large absorption coefficient (>10^5 cm^{-1}), decent

carrier mobility (~10 $cm^2V^{-1}s^{-1}$) and long carrier lifetime (~60 ns).[9-11] Furthermore, Sb_2Se_3 possesses advantages of low-toxicity, low-cost and earth-abundant constitutes, the only one stable crystalline phase can also get rid of complex composition and secondary phase control during thin film deposition process. According to theoretical calculations, the PCE of Sb_2Se_3 can be as high as 30%, further strength its competitiveness as a new photovoltaic material.[12,13]

Great progress for Sb_2Se_3 solar cells has been achieved in the last decade, obtaining the current efficiency record of 3.21% for Sb_2Se_3 mesoporous sensitized-type,[14] 7.62% for planar heterojunction geometry-type[15] and the highest 9.2% for core-shell structured Sb_2Se_3 nanorod array solar cells.[16] By comparison, planar heterojunction Sb_2Se_3 solar cells are proven to have better performances than sensitized mesoporous solar cells because of the diversity of substrates, the tunability of interfaces and various deposition methods for the absorber layer. Sb_2Se_3 absorbing films have been successfully prepared using various methods such as electrochemical deposition,[17] solution processing,[18] thermal (or rapid thermal) evaporation,[19,20] closed-space sublimation,[21] vapor transport deposition[10] and the magnetron sputtering.[22] Among these methods, magnetron sputtering can be considered as an effective deposition technique with distinct advantages like full-vacuum operation, accurate composition transfer from targets to films, good uniformity over large areas and competitive industrial scale-up. Our group has made great efforts to prepare Sb_2Se_3 thin film solar cells via magnetron sputtering and recently achieved an interesting PCE of 6.06% as well as a highest V_{OC} value of 494 mV.[22-24] Sb_2Se_3 thin film prepared by magnetron

sputtering combined with post-selenization has benign growth orientation, accurate chemical composition and reduced deep level defect density. Despite these endeavors, as an important part, the studies on the sputtering target are rarely reported, especially the concern to construct a facile and versatile path for targets preparation. Compared with the commercial sputtering targets, the homemade targets could have many advantages, such as reducing the cost significantly, tailoring the chemical composition independently and realizing pristine doping efficiently, thus needs further investigation.

In this work, an effective method of ball milling followed with spark plasma sintering (SPS) was used to prepare high-quality Sb_2Se_3 sputtering target. Then the Sb_2Se_3 absorbing thin films have been prepared by using radio frequency (RF) magnetron sputtering with an additional post-selenization heat treatment. A champion Sb_2Se_3 thin film solar cell with substrate configuration of Mo/Sb_2Se_3/CdS/ITO/Ag can achieve an interesting PCE of 5.08%. The combined features of homemade sputtering target and advantageous thin film preparation further demonstrated its attractive potential for thin film photovoltaic applications.

2. Experimental details

2.1. Preparation of Sb_2Se_3 target

An effective method of ball milling combined with SPS process using 30 g of high purity Sb_2Se_3 particles (99.99%, Advanced Material Professional Manufacture, 100 meshes) as raw materials was used to prepare Sb_2Se_3 target. A schematic illustration of the preparation process is shown in Fig. 1. The ball milling was performed at room

temperature in a vertical planetary ball mill using hardened steel balls and stainless steel cell, after 6 hours with a speed of 300 rpm/min, fine Sb_2Se_3 powder can be obtained. The SPS process was carried out by using an apparatus Labox-325 SPS. The as-milled Sb_2Se_3 powder was placed inside a graphite die of 60 mm diameter and covered with a thin carbon layer. A fixed pressure of 30 KN was applied before running the two-step heating procedures, specifically, increasing the temperature from room temperature to 300 °C with a heating rate of 20 °C/min firstly and then further increasing to 420 °C with a slower rate of 10 °C/min. After 5 min dwell, the electric current was turned off, the pressure was released and the sample was cooled down to room temperature. Finally, the bulk sample was taken out and the surface was finely polished to obtain a qualified homemade magnetron sputtering target with diameter of 60 mm and a thickness of approximately 2 mm. The target was closely bonded onto a copper backing plate using indium in order to improve its heat dissipation ability.

2.2 Preparation of Sb_2Se_3 thin film solar cell

Sb_2Se_3 thin films were prepared by using RF magnetron sputtering involved with post-selenization heat treatment, as depicted in Fig. 1. Based on the homemade Sb_2Se_3 target, Mo-coated soda lime glass was chosen as device substrate. Prior to sputtering, it was ultrasonically cleaned in sequential detergent, acetone, isopropanol and ethanol solution for 10 min, respectively. The chamber was evacuated to a residual pressure of less than 8.0×10^{-4} Pa before each deposition. Argon gas was introduced at a rate of 40 sccm and the deposition was carried out with a fixed power of 35 W also with a relatively low pressure of 1.0 Pa. The deposition time was 90 min with an

approximate rate of 10 nm/min. After that, a post-selenization heat treatment was applied in order to eliminate the possible detrimental selenium vacancies and obtain crystalline Sb_2Se_3 thin films. In detail, high purity Se particles (99.999%, particle size: 1-6 mm, Aladdin) and the as-deposited thin film were separately placed into a double-chamber vacuum tubular furnace. The furnace was evacuated by using a mechanical pump and high purity argon gas was then introduced to maintain working pressure of 5×10^4 Pa. Temperature of the Se side was fixed at 400 °C to provide sufficient Se partial pressure, selenization of the thin films was last for 20 min at temperatures of 380 °C, 400 °C, 420 °C and 440 °C, respectively. All those temperatures were ramped to the setting values at a rate of 20 °C/min.

After the preparation of Sb_2Se_3 thin film, CdS buffer layer was then deposited via chemical bath deposition method, an additional heat treatment at 300 °C for 5 min in argon atmosphere was used to induce elemental inter-diffusion and optimize the band alignment. Indium tin oxide (ITO) window layer was subsequently deposited using direct current (DC) magnetron sputtering under a power of 60 W, a pressure of 0.4 Pa and a flow rate of 30 sccm for argon and oxygen gas, respectively. Finally, the device surface was scribed into small squares with identical area and then low-temperature (60 °C) solidified Ag colloids were painted onto the surface to form metallic contact. Sb_2Se_3 solar cell with substrate structure of Mo/Sb_2Se_3/CdS/ITO/Ag was prepared and used for performance measurements under an active device area of 0.15 cm^2.

2.3 Characterizations

The crystal structure of Sb_2Se_3 thin films were characterized by X-ray diffraction

(XRD, Ultima-IV) with CuK_{α} radiation under 40 kV and 40 mA. Morphologies of the thin films were observed using a Zeiss SUPRA 55 thermal field emission scanning electron microscope (SEM). A SEM-coupled Energy Dispersive X-ray Spectroscope (EDS, BRUKER QUANTAX 200) was also used to analyze the chemical compositions and the elemental distribution. Transmission electron microscope (TEM) measurements were performed on a FEI Titan Cubed Themis G2 300 microscope, the sample was prepared by ablating the single thin film solar cell using focused ion beam (FIB, FEI Scios). A Shimadzu UV-3600 UV/Vis/NIR spectrophotometer equipped with monochromator was used for the optical reflectance and transmittance investigation and using pure soda-lime glass as the substrate. Current density-voltage (J-V) curves were measured by using a multi-meter (Keithley, 2400 Series) under AM 1.5G light illumination from a 3A solar simulator with intensity calibrated to 100 mW/cm^2 through a Si reference cell. The voltage was forwardly and backwardly scanned from -0.1 V to 0.6 V with a scan rate of 0.01 V/s. The external quantum efficiency (EQE) spectra were obtained using a Zolix SCS101 system with a monochromator and a Keithley 2400 source meter.

3. Results and Discussion

Fig. 2a shows the XRD patterns of the pristine commercial Sb_2Se_3 powder, the powder after ball milling and the as-prepared target after SPS. It can be seen that all the diffraction peaks match well with the JCPDS standard card (No. 15-0861) of the orthorhombic phase of Sb_2Se_3 without any detectable impurities. Compared with pristine Sb_2Se_3 powder, the absence of localized broad peak (17°-27°) of the

ball-milled powder indicates a slight improvement of crystallinity due to the elimination of some amorphous particles under low-energy treatment. Moreover, the ball milling induced crystal size decrease can also be observed. According to the Scherrer equation, $Dp=0.94\lambda/\beta_{1/2}\cos\theta$, where Dp is crystal size, λ is wavelength, $\beta_{1/2}$ is the full-width at half-maximum (FWHM) and θ is the peak position.[25] Two major peaks of (221) and (240) figure out crystal size of 3.17 nm and 3.36 nm for the pristine powder, respectively. Then the values decrease to 2.25 nm and 2.90 nm after ball milling. The obtained finer powder with higher crystallinity is really beneficial for preparing high-quality Sb_2Se_3 target. The XRD pattern of the Sb_2Se_3 target also presents a modified preferential crystallographic orientation from (240) to (221) after SPS, which is reasonable to occur under the coaction of the pulsed electric current and the applied pressure.[26] Importantly, the special heating mechanism of SPS makes this technology capable of sintering Sb_2Se_3 target at a lower temperature (420 °C), a faster heating rate (20 °C/min) and a shorter sintering time (5 min) than those of the conventional sintering technologies. Furthermore, the obtained target has a rather ideal relative density as high as 98% measured by using Archimedes drainage method.[27] As shown in Fig. 2b, the polished Sb_2Se_3 target has flat and smooth surface without obvious cracks or holes. The representative cross-sectional SEM images of the target further confirm its highly dense and compact nature with a thickness approaching to 2 mm. Overall, the as-prepared target by ball milling and SPS meets the criteria for subsequent magnetron sputtering.

Fig. 3a presents the XRD patterns of the as-deposited and post-selenized Sb_2Se_3

thin films at different temperatures. For the as-deposited thin film, no diffraction peaks correspond to the crystalline phase can be observed except a single peak (2θ=41°) belonging to Mo substrate, suggesting its amorphous nature. Afterwards, the thin film was annealed under selenium atmosphere (post-selenization) at four different temperatures of 380 °C, 400 °C, 420 °C and 440 °C, respectively. The XRD patterns of these post-selenized thin films exhibit prominent peaks in good agreement with the JCPDS standard card (No. 15-0861) of the orthorhombic phase of Sb_2Se_3. A slight increase of peak intensities with increasing the post-selenization temperature to 420 °C suggests the crystallinity improvement of the Sb_2Se_3 thin films upon annealing. Moreover, three major diffraction peaks of (211), (221) and (301) show sharp characteristics, indicating the highly crystalline nature, also with a preferential growth orientation of (hk1). Plenty of studies have pointed out that such perpendicular growth of the Sb_2Se_3 grains would reduce the recombination loss at grain boundaries, promote the carrier transport throughout absorber layer, thus improving the device performance.[15,20,28] However, once an excessively high selenization temperature (440 °C) was applied, the diffraction peak intensities of the Sb_2Se_3 thin film with observable decrease was possibly due to its decomposition.

Fig. 3b-f presents the top-view SEM images of the as-prepared thin films. As shown in Fig. 3b, no obvious crystal grains can be observed for the as-deposited amorphous thin film. Fine particles were formed on the substrate due to the limited mobility of Sb_2Se_3 molecules and weak surface diffusion during the sputtering process. The highly compact nature was also closely related to its low deposition

pressure (1.0 Pa) according to the Thornton magnetron sputtering regional structure model at substrate temperature and Sb_2Se_3 melting temperature ratio Ts/Tm of 0.34.[29] After post-selenized at 380 °C, the molecules were diffused under thermal motion and rearranged to form micron-sized Sb_2Se_3 crystal grains. The existence of some pinholes on the surface can be attributed to the insufficient crystallization and growth process (Fig. 3c), consistent with the XRD result. Further increasing the post-selenization temperature to 400 °C and 420 °C, it leads to a more dense and uniform crystalline thin film accompanied by columnar growth of ellipsoid grains with an average size of approximately 750 nm, which is advantageous for suppress the recombination loss at the grain boundaries. However, if the temperature is too high, e.g., 440 °C, as depicted in Fig. 3f, though some crystal grains become larger, thermal induced the formation of distinct micro-voids due to Se evaporated from the as-deposited Sb_2Se_3 thin film under its high vapor pressure nature, which could produce shunt paths and cause severe current leakage. Therefore, it is crucial to control the post-selenization temperature to obtain high-quality Sb_2Se_3 absorber layer with high crystallinity and benign growth orientation.

The elemental composition of the as-prepared target, as-deposited thin film and the post-selenized thin films were obtained from SEM-coupled EDS analysis. As shown in Table 1, the Sb_2Se_3 target has a slight Se poor with Sb/Se ratio of 0.72 and it possibly occurred due to the applied energy and/or heat during ball-milling and SPS processes. The as-deposited amorphous thin film has a quite similar composition with the target, confirming an accurate composition transfer character for this

advantageous RF magnetron sputtering. An additional post-selenization heat treatment was designed to induce crystallization and also compensate the pristine Se loss. As expected, the post-selenized crystalline thin films show an overall increased Se content, an optimal ratio of 0.66 obtained at 420 °C is close to the standard stoichiometric ratio of 0.67 for Sb_2Se_3. Moreover, the decreased Se content at 440 °C is also consistent with the SEM observations under the existence of Se-deficit micro-voids.

To investigate the optical properties of the as-prepared Sb_2Se_3 thin films, UV/Vis/NIR spectrophotometer has been performed to obtain the reflection and transmission spectra of the thin films using glass as substrate and covering a range from 300 nm to 1500 nm. As shown in Fig. 4a and Fig. 4b, a prominent difference of reflectance and transmittance between the amorphous thin film and crystalline Sb_2Se_3 thin films can be observed, which can be assigned to an intrinsic evolution of the atomic arrangement changed from disorder to order. The obvious red-shift of the absorption region observed in reflection spectra, accompanied by the synchronous red-shift of the short wavelength cut-off edge from 700 nm for the amorphous thin film to about 860 nm for the crystalline thin film, both clearly imply the variation of band gap. To specify the real value, it can be calculated according to the following formulas:

$$\alpha = \frac{1}{d}\ln\left(\frac{1-R(\lambda)}{T(\lambda)}\right) \quad (1)$$

$$\alpha h\nu = C(h\nu - E_g)^n \quad (2)$$

where α is the absorption coefficient, d is the thickness, R and T are the reflectance

and transmittance, respectively.[30] The latter is a typical Tauc formula, where C is a constant, h is the Planck's constant, v is the photon frequency, n is an index defined by 0.5 for direct and 2.0 for indirect bandgap semiconductor.[31] The as-deposited amorphous thin film has a direct band gap of 1.68 eV, then the post-selenization induced the value decrease to 1.33 eV, 1.29 eV, 1.27 eV and 1.19 eV for the Sb_2Se_3 thin films underwent 380 °C, 400 °C, 420 °C and 440 °C heat treatment, respectively. Notably, the calculated band gap agree well with that given in prior publications for crystalline Sb_2Se_3 thin films.[23] Moreover, the optimal Sb_2Se_3 thin film post-selenized at 420 °C with a band gap of 1.27 eV can be considered as an efficient absorber layer in thin film photovoltaic applications.

Compared with the widely investigated superstrate Sb_2Se_3 thin film solar cells, the solar cells with substrate configuration have many advantages, such as tailoring the absorber layer independently, engineering the interface efficiently and fabricating flexible or tandem solar cells facile.[32] Herein, Sb_2Se_3 thin film solar cell with substrate structure of Mo/Sb_2Se_3/CdS/ITO/Ag was prepared and a schematic illustration of this device is shown in Fig. 5a. The representative cross-sectional SEM image of the device (Fig. 5b) displays obvious layered structure with approximate thickness of 850 nm, 60 nm and 500 nm for Sb_2Se_3, CdS and ITO layer, respectively. The Sb_2Se_3 absorber layer is consisted of large crystal grains with columnar growth. The interface between Sb_2Se_3 and CdS also shows compact, well-adherent and pinhole-free characteristics, which is beneficial for reducing charge carrier recombination and current leakage. Furthermore, the corresponding EDS elemental

mappings marked with Mo, Sb, Se, Cd, S and In are also conducted to confirm the compositional distribution. Elements of Sb and Se present good uniformity throughout the whole Sb_2Se_3 absorber layer, confirming the high quality of this post-selenized Sb_2Se_3 thin film. Notably, an observable Cd inter-diffusion is reasonable to occur because of the additional post-annealing of the device, which has been reported to be beneficial for obtaining favorable band alignment and reducing the recombination at the heterojunction interfaces.[33]

Fig. 6 shows the champion device performances based on the Sb_2Se_3 thin film post-selenized at 420 °C. According to the current density-voltage (J-V) curve (Fig. 6a), under the simulated AM1.5G solar irradiation, the device offers a short-circuit current density (J_{SC}) of 23.0 mA/cm^2, an open circuit voltage (V_{OC}) of 480 mV, and a fill factor (FF) of 46.0%, thus achieving a power conversion efficiency of 5.08%. In addition, no obvious hysteresis between the forward (J_{SC} to V_{OC}) and backward (V_{OC} to J_{SC}) scans can be observed in our device, suggesting the high-quality Sb_2Se_3 absorber layer and the reasonable substrate device configuration.[34] Importantly, the obtained device performances are comparable to that of state-of-the-art Sb_2Se_3 thin film solar cells.[11,24,35] As shown in Fig. 6b, the external quantum efficiency (EQE) spectrum reveals the photo-response covering a broad UV-visible-NIR range, which agrees well with the narrow band gap of Sb_2Se_3. The maximum value can reach higher than 80%, implying less recombination losses at the well-adherent Sb_2Se_3/CdS interface as well as in the bulk absorber layer. Wherein, the as-prepared Sb_2Se_3 thin film with high crystallinity and advantageous preferential orientation can effectively

induce bulk defects passivation. Finally, the integrated J_{SC} calculated from EQE data is also drawn in Fig. 6b, a value of 20.8 mA/cm^2 is comparable to the J-V measurement result.

To further confirm the high quality of Sb_2Se_3/CdS interface as well as the Sb_2Se_3 absorber layer, morphological and structural characterizations of the champion device by TEM are shown in Fig. 7. The existence of layered structure with specific thickness is consistent with SEM results (Fig. 7a). High-resolution TEM (HRTEM) analysis was performed at the Sb_2Se_3/CdS interface, though it is not exactly epitaxial growth of CdS on the Sb_2Se_3 layer due to their lattice mismatch, a smooth and adherent interface can be observed, corresponding to the elemental inter-diffusion. The absence of crystal lattice distortion or amorphous layer at the interface region further demonstrates its efficient generation and separation of photo-carriers. Afterwards, HRTEM images correspond to three arbitrary points 1, 2 and 3 that were randomly selected near the top, middle and bottom regions of the Sb_2Se_3 absorber layer were measured, as shown in Fig. 7c-e. All the three points show quite similar lattice fringes with interplanar d-spacings of approximately 0.289 nm and 0.316 nm that agree well with the distance of the (221) and (211) lattice planes of the orthorhombic phase Sb_2Se_3. This preferential growth is consistent with its pristine target and closely related to a proper post-selenization treatment. According to the recent theoretical and experimental studies, it is indeed determined intrinsically by the anisotropic Sb-Se atom chain and layer structure of Sb_2Se_3.[36,37] Furthermore, such a vertical crystal growth orientation across the whole Sb_2Se_3 thin film will greatly

facilitate charge carrier transport within the absorber layer and thus improving the final device performance.

4. Conclusions

In summary, a facile method of ball milling combined with SPS process has been successfully developed to prepare compact and dense Sb_2Se_3 target with smooth surface. Sb_2Se_3 thin films can be prepared by RF magnetron sputtering using the homemade target also with an additional post-selenization heat treatment at different temperatures. The as-deposited thin film shows amorphous nature and then the highly crystalline thin film consisted of large crystal grains can be obtained after post-selenization treatment. A systematic investigation of temperature-induced crystallization, preferential orientation, stoichiometric ratio variation, surface morphologies evolution and optical properties modification conclude an optimal post-selenization temperature of 420 °C. Efficient Sb_2Se_3 thin film solar cell with substrate structure of Mo/Sb_2Se_3/CdS/ITO/Ag was fabricated. The champion device with highly interesting PCE of 5.08% (J_{SC}=23.0 mA/cm^2, V_{OC}=480 mV, FF=46.0%) and maximum EQE value higher than 80% has been achieved. Further morphological and structural characterizations confirm the positive effects of proper preferential orientation of the Sb_2Se_3 absorber layer and smooth contact of the Sb_2Se_3/CdS heterojunction interface on such superior device performances.

Acknowledgements

G. Liang and R. Tang contributed equally. This work was supported by Key Project of

Department of Education of Guangdong Province (No. 2018KZDXM059), Science and Technology plan project of Shenzhen (20190726221232961), National Natural Science Foundation of China (No. 61404086 and 51802050), The Natural Science Foundation of Guizhou Province (Qian Ke He [2017]1064), Shenzhen Key Lab Fund (ZDSYS 20170228105421966). The authors wish to acknowledge the assistance on HAADF-STEM observation received from the Electron Microscope Center of the Shenzhen University.

References

[1] A. Hussain, S. M. Arif, M. Aslam, Emerging renewable and sustainable energy technologies: State of the art. *Renewable Sustainable Energy Rev.* 2017, *71*, 12-28.

[2] M. K. Nazeeruddin, In Retrospect Twenty-five years of low-cost solar cells. *Nature* 2016, *538*, 463-464.

[3] H. Lei, J. Chen, Z. Tan, G. Fang, Review of Recent Progress in Antimony Chalcogenide-Based Solar Cells: Materials and Devices. *Solar RRL* 2019, 1900026.

[4] A. Polman, M. Knight, E. C. Garnett, B. Ehrler, W. C. Sinke, Photovoltaic materials: Present efficiencies and future challenges. *Science* 2016, *352*, 4424-4424.

[5] H. Savin, P. Repo, G. von Gastrow, P. Ortega, E. Calle, M. Garin, R. Alcubilla, Black silicon solar cells with interdigitated back-contacts achieve 22.1% efficiency. *Nat. Nanotechnol.* 2015, *10*, 624-628.

[6] R. Carron, S. Nishiwaki, T. Feurer, R. Hertwig, E. Avancini, J. Lockinger, S. C. Yang, S. Buecheler, A. N. Tiwari, Advanced Alkali Treatments for High-Efficiency Cu(In,Ga)Se_2 Solar Cells on Flexible Substrates. *Adv. Energy Mater.* 2019, *9*, 1900408.

[7] J. M. Burst, J. N. Duenow, D. S. Albin, E. Colegrove, M. O. Reese, J. A. Aguiar, C. S. Jiang, M. K. Patel, M. M. Al-Jassim, D. Kuciauskas, S. Swain, T. Ablekim, K. G. Lynn, W. K. Metzger, CdTe solar cells with open-circuit voltage breaking the 1V

barrier. *Nat. Energy* 2016, *1*, 16015.

[8] C. Chen, K. H. Li, S. Y. Chen, L. Wang, S. C. Lu, Y. H. Liu, D. B. Li, H. S. Song, J. Tang, Efficiency Improvement of Sb_2Se_3 Solar Cells via Grain Boundary Inversion. *ACS Energy Lett.* 2018, *3*, 2335-2341.

[9] D. B. Li, X. X. Yin, C. R. Grice, L. Guan, Z. N. Song, C. L. Wang, C. Chen, K. H. Li, A. J. Cimaroli, R. A. Awni, D. W. Zhao, H. S. Song, W. H. Tang, Y. F. Yan, J. Tang, Stable and efficient CdS/Sb_2Se_3 solar cells prepared by scalable close space sublimation. *Nano Energy* 2018, *49*, 346-353.

[10] X. Wen, C. Chen, S. Lu, K. Li, R. Kondrotas, Y. Zhao, W. Chen, L. Gao, C. Wang, J. Zhang, G. Niu, J. Tang, Vapor transport deposition of antimony selenide thin film solar cells with 7.6% efficiency. *Nat. Commun.* 2018, *9*, 2179.

[11] L. Wang, D. B. Li, K. Li, C. Chen, H. X. Deng, L. Gao, Y. Zhao, F. Jiang, L. Li, F. Huang, Y. He, H. Song, G. Niu, J. Tang, Stable 6%-efficient Sb_2Se_3 solar cells with a ZnO buffer layer. *Nat. Energy* 2017, *2*, 17046.

[12] C. Chen, L. Wang, L. Gao, D. Nam, D. Li, K. Li, Y. Zhao, C. Ge, H. Cheong, H. Liu, H. Song, J. Tang, 6.5% Certified Efficiency Sb_2Se_3 Solar Cells Using PbS Colloidal Quantum Dot Film as Hole-Transporting Layer. *ACS Energy Lett.* 2017, *2*, 2125-2132.

[13] C. Ou, K. Shen, Z. Li, H. Zhu, T. Huang, Y. Mai, Bandgap tunable CdS:O as efficient electron buffer layer for high-performance Sb_2Se_3 thin film solar cells. *Sol. Energy Mater. Sol. Cells* 2019, *194*, 47-53.

[14] Y. C. Choi, T. N. Mandal, W. S. Yang, Y. H. Lee, S. H. Im, J. H. Noh, S. I. Seok, Sb_2Se_3-Sensitized Inorganic-Organic Heterojunction Solar Cells Fabricated Using a Single-Source Precursor. *Angew. Chem., Int. Ed.* 2014, *53*, 1329-1333.

[15] K. Li, C. Chen, S. Lu, C. Wang, S. Wang, Y. Lu, J. Tang, Orientation Engineering in Low-Dimensional Crystal-Structural Materials via Seed Screening. *Adv. Mater.* 2019, *31*, 1903914.

[16] Z. Li, X. Liang, G. Li, H. Liu, H. Zhang, J. Guo, J. Chen, K. Shen, X. San, W. Yu, R. E. I. Schropp, Y. Mai, 9.2%-efficient core-shell structured antimony selenide nanorod array solar cells. *Nat. Commun.* 2019, *10*.

[17] T. T. Ngo, S. Chavhan, I. Kosta, O. Miguel, H. J. Grande, R. Tena-Zaera, Electrodeposition of Antimony Selenide Thin Films and Application in Semiconductor Sensitized Solar Cells. *ACS Appl. Mater. Interfaces* 2014, *6*, 2836-2841.

[18] Y. Zhou, M. Y. Leng, Z. Xia, J. Zhong, H. B. Song, X. S. Liu, B. Yang, J. P. Zhang, J. Chen,; K. H. Zhou, J. B. Han, Y. B. Cheng, J. Tang, Solution-Processed Antimony Selenide Heterojunction Solar Cells. *Adv. Energy Mater.* 2014, *4*, 1301846.

[19] M. Luo, M. Y. Leng, X. S. Liu, J. Chen, C. Chen, S. K. Qin, J. Tang, Thermal evaporation and characterization of superstrate CdS/Sb_2Se_3 solar cells. *Appl. Phys. Lett.* 2014, *104*, 173904.

[20] Y. Zhou, L. Wang, S. Y. Chen, S. K. Qin, X. S. Liu, J. Chen, D. J. Xue, M. Luo, Y. Z. Cao, Y. B. Cheng, E. H. Sargent, J. Tang, Thin-film Sb_2Se_3 photovoltaics with oriented one-dimensional ribbons and benign grain boundaries. *Nat. Photonics* 2015, *9*, 409-415.

[21] L. P. Guo, B. Y. Zhang, Y. Qin, D. W. Li, L. Li, X. F. Qian, F. Yan, Tunable Quasi-One-Dimensional Ribbon Enhanced Light Absorption in Sb_2Se_3 Thin-film Solar Cells Grown by Close-Space Sublimation. *Sol. RRL* 2018, *2*, 1800128.

[22] G. X. Liang, Z. H. Zheng, P. Fan, J. T. Luo, J. G. Hu, X. H. Zhang, H. L. Ma, B. Fan, Z. K. Luo, D. P. Zhang, Thermally induced structural evolution and performance of Sb_2Se_3 films and nanorods prepared by an easy sputtering method. *Sol. Energy Mater. Sol. Cells* 2018, *174*, 263-270.

[23] S. Chen, Z. Zheng, M. Cathelinaud, H. Ma, X. Qiao, Z. Su, P. Fan, G. Liang, X. Fan, X. Zhang, Magnetron sputtered Sb_2Se_3-based thin films towards high performance quasi-homojunction thin film solar cells. *Sol. Energy Mater. Sol. Cells* 2019, *203*, 110154.

[24] R. Tang, Z. H. Zheng, Z. H. Su, X. J. Li, Y. D. Wei, X. H. Zhang, Y. Q. Fu, J. T. Luo, P. Fan, G. X. Liang, Highly efficient and stable planar heterojunction solar cell based on sputtered and post-selenized Sb_2Se_3 thin film. *Nano Energy* 2019, *64*, 103929.

[25] P. Ramakrishnan, S. H. Baek, Y. Park, J. H. Kim, Nitrogen and sulfur co-doped

metal monochalcogen encapsulated honeycomb like carbon nanostructure as a high performance lithium-ion battery anode material. *Carbon* 2017, *115*, 249-260.

[26] F. Balima, F. Bellin, D. Michau, O. Viraphong, A. Poulon-Quintin, U. C. Chung, A. Dourfaye, A. Largeteau, High pressure pulsed electric current activated equipment (HP-SPS) for material processing. *Mater. Des.* 2018, *139*, 541-548.

[27] M. Zhou, L. Xu, X. Xi, P. Li, W. Dai, W. Zhu, A. Shui, L. Zeng, Investigation on the preparation and properties of monodispersed Al_2O_3-ZrO_2 nanopowder via Co-precipitation method. *J. Alloys Compd.* 2016, *678*, 337-342.

[28] J. Tao, X. Hu, Y. Guo, J. Hong, K. Li, J. Jiang, S. Chen, C. Jing, F. Yue, P. Yang, C. Zhang, Z. Wu, J. Tang, J. Chu, Solution-processed SnO_2 interfacial layer for highly efficient Sb_2Se_3 thin film solar cells. *Nano Energy* 2019, *60*, 802-809.

[29] W. J. Meese, T. M. Lu, Scaling behavior of columnar structure during physical vapor deposition. *J. Appl. Phys.* 2018, *123*, 075302.

[30] T. Kobayashi, T. Kumazawa, Z. J. L. Kao, T. Nakada,, Cu(In,Ga)Se_2 thin film solar cells with a combined ALD-Zn(O,S) buffer and MOCVD-ZnO:B window layers. *Sol. Energy Mater. Sol. Cells* 2013, *119*, 129-133.

[31] L. Li, G. Li, T. Zhang, C. Lin, G. Wang, S. Dai, Q. Nie, Q. Jiao, Preparation and properties of Ge-Ga-La-S-AgI chalcogenide glass. *Ceram. Int.* 2017, *43*, 4508-4512.

[32] G. Pan, D. Wang, S. Gao, P. Gao, Q. Sun, X. Liu, Z. Zhou, Y. Sun, Y. Zhang, Substrate structured Sb_2S_3 thin film solar cells fabricated by rapid thermal evaporation method. *Sol. Energy* 2019, *182*, 64-71.

[33] C. Yan, J. Huang, K. Sun, S. Johnston, Y. Zhang, H. Sun, A. Pu, M. He, F. Liu, K. Eder, L. Yang, J. M. Cairney, N. J. Ekins-Daukes, Z. Hameiri, J. A. Stride, S. Chen, M. A. Green, X. Hao, Cu_2ZnSnS_4 solar cells with over 10% power conversion efficiency enabled by heterojunction heat treatment. *Nat. Energy* 2018, *3*, 764-772.

[34] S. C. Liu, Y. Yang, Z. Li, D. J. Xue, J. S. Hu, GeSe thin-film Solar Cells. *Mater. Chem. Front.* 2020, DOI: 10.1039/c9qm00727j.

[35] X. Hu, J. Tao, Y. Wang, J. Xue, G. Weng, C. Zhang, S. Chen, Z. Zhu, J. Chu, 5.91%-efficient Sb_2Se_3 solar cells with a radio-frequency magnetron-sputtered CdS buffer layer. *Appl. Mater. Today* 2019, *16*, 367-374.

[36] S. Chen, X. S. Qiao, F. X. Wang, Q. Luo, X. H. Zhang, X. Wan, Y. Xu, X. P. Fan, Facile synthesis of hybrid nanorods with the $Sb_2Se_3/AgSbSe_2$ heterojunction structure for high performance photodetectors. *Nanoscale* 2016, *8*, 2277-2283.

[37] C. Chen, D. C. Bobela, Y. Yang, S. Lu, K. Zeng, C. Ge, B. Yang, L. Gao, Y. Zhao, M. C. Beard, J. Tang, Characterization of basic physical properties of Sb_2Se_3 and its relevance for photovoltaics. *Front. Optoelectron.* 2017, *10*, 18-30.

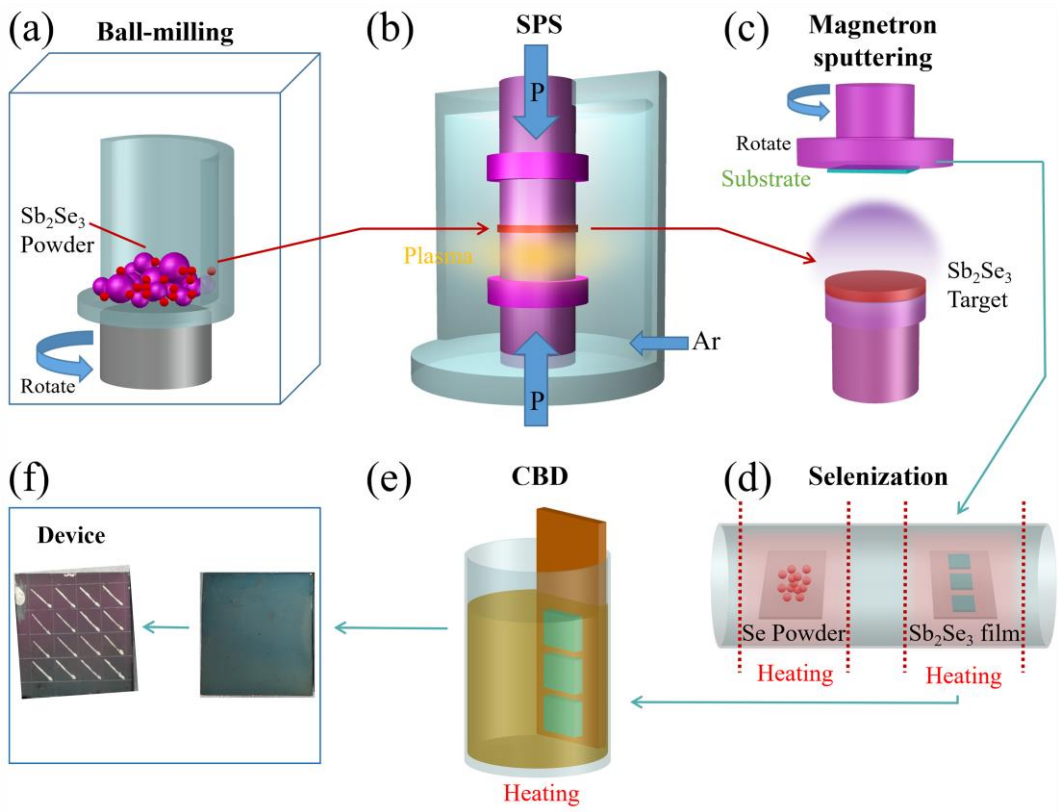

Fig. 1. Schematic illustration of the preparation process of the substrate structured Sb_2Se_3 thin film solar cells. (a) Sb_2Se_3 fine powder obtained by ball milling, (b) Sb_2Se_3 target obtained by SPS process, (c) Sb_2Se_3 thin film deposition by RF magnetron sputtering, (d) Post-selenization heat treatment, (e) CdS buffer layer deposition via CBD method, (f) Representative photographs of the device, surface morphologies of device after ITO layer deposited and Ag electrodes painted.

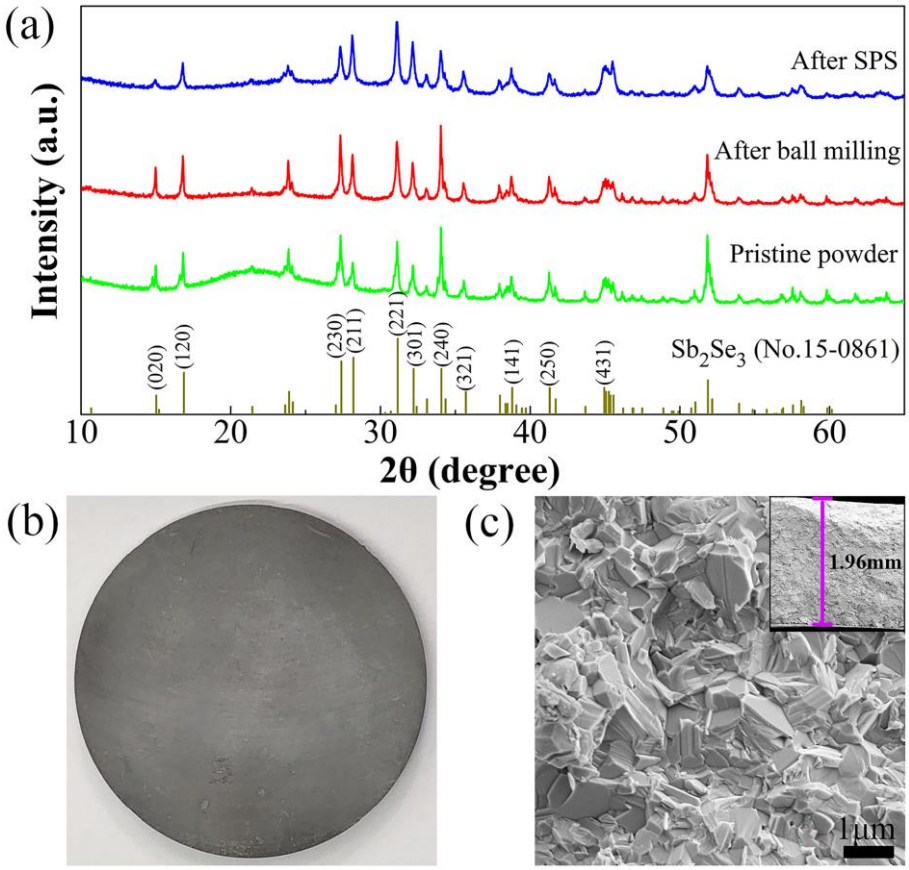

Fig. 2. (a) XRD patterns of the pristine commercial Sb_2Se_3 powder, the powder after ball milling and the as-prepared target after SPS, (b) Surface morphology and (c) Cross-sectional SEM images of the Sb_2Se_3 target.

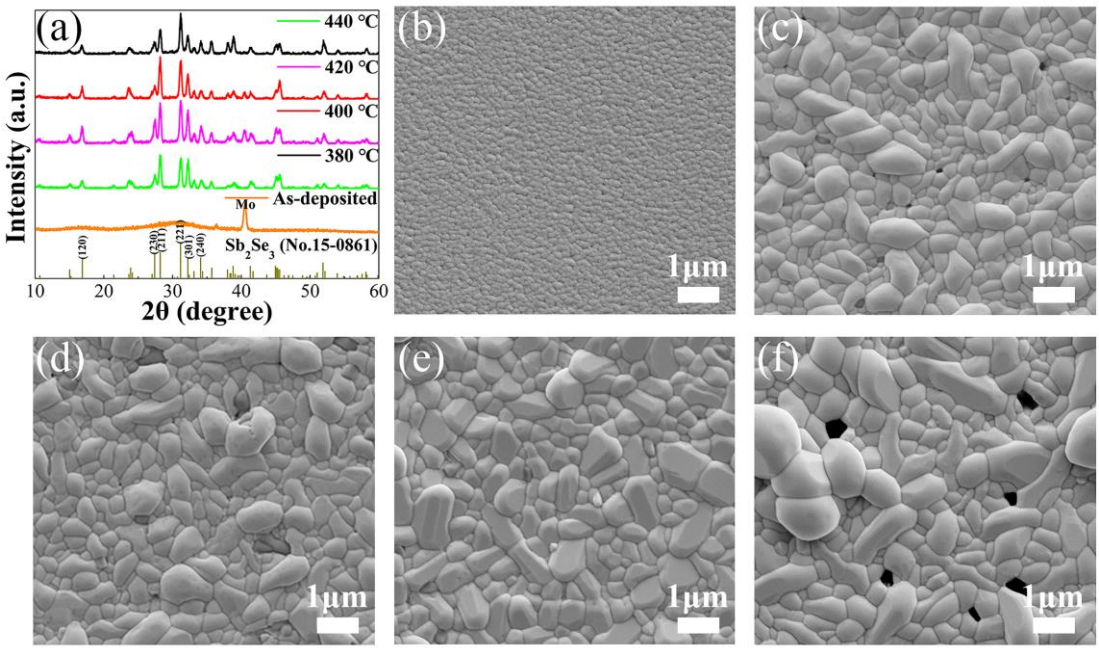

Fig. 3. Characterizations of the Sb_2Se_3 thin films post-selenized at different temperatures: (a) XRD patterns, (b-f) Top-view SEM images of the thin films post-selenized at temperatures of (b) as-deposited, (c) 380 ℃, (d) 400 ℃, (e) 420 ℃ and (f) 440 ℃.

Table 1. Elemental composition of the Sb_2Se_3 target and Sb_2Se_3 thin films obtained from EDS analysis

Element	Target	As-deposited	380 ℃	400 ℃	420 ℃	440 ℃
Sb (at%)	41.9	41.77	40.80	38.77	39.91	42.58
Se (at%)	58.1	58.23	59.20	61.23	60.09	57.42
Sb/Se	0.72	0.72	0.69	0.63	0.66	0.74

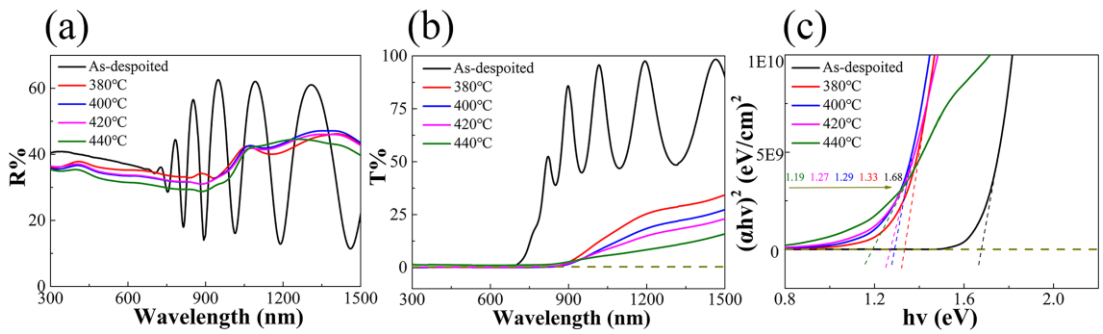

Fig. 4. Optical characterizations of the Sb_2Se_3 thin films as a function of wavelength and with different post-selenization temperatures. (a) Reflection spectra, (b) Transmission spectra and (c) Plot of $(\alpha h\nu)^2$ versus $h\nu$, used to obtain direct band gap.

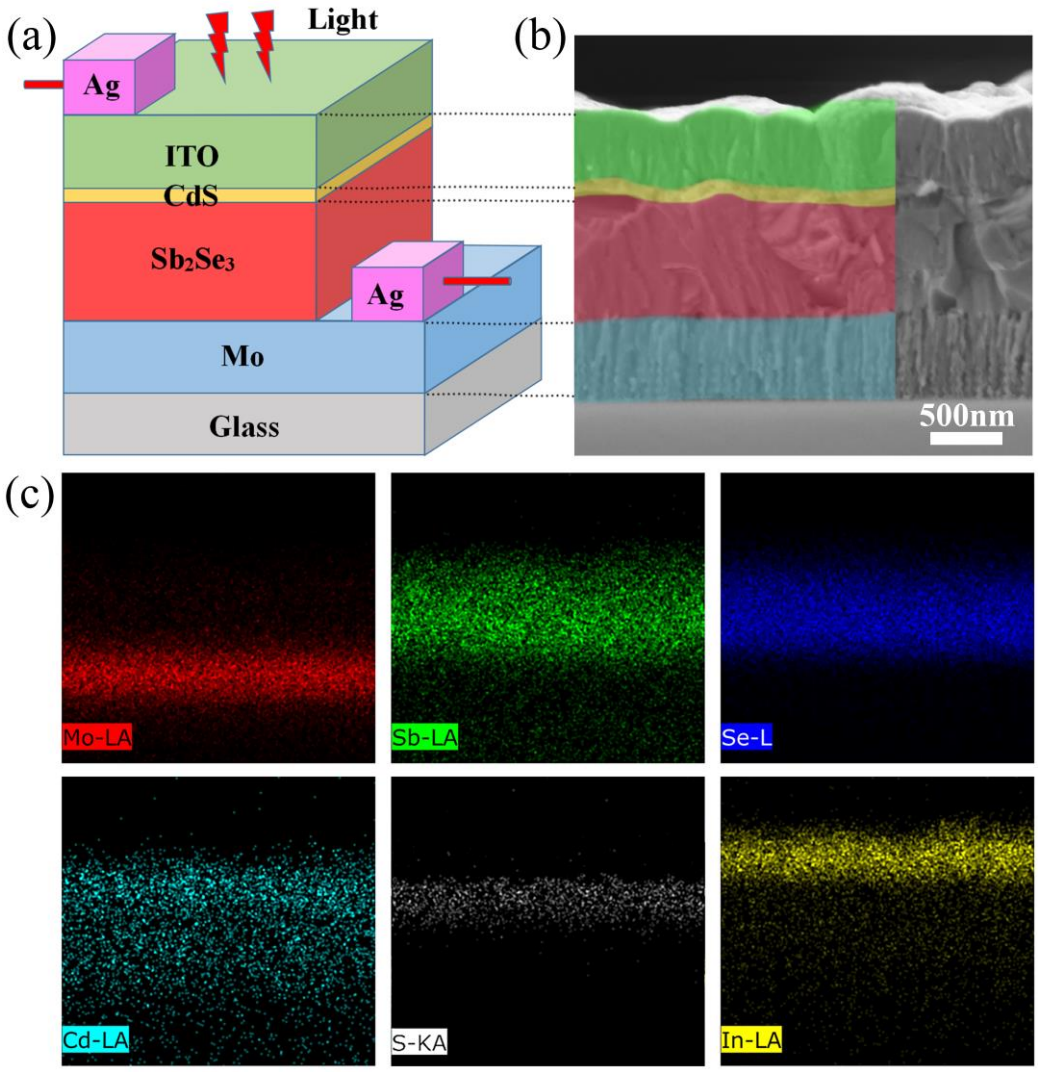

Fig. 5. (a) Schematic configuration of the Sb_2Se_3 thin film solar cell. (b) Cross-sectional SEM image of the device and (c) the corresponding EDS elemental mappings of Mo, Sb, Se, Cd, S and In, used to reveal the compositional distribution.

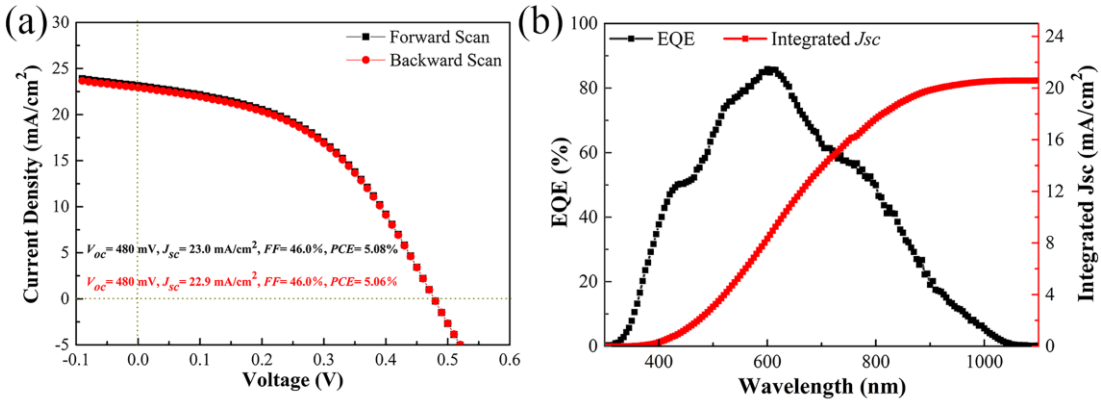

Fig. 6. J-V curves of the champion Sb_2Se_3 thin film solar cell under forward scan and backward scan. (b) EQE and integrated J_{sc} of the device.

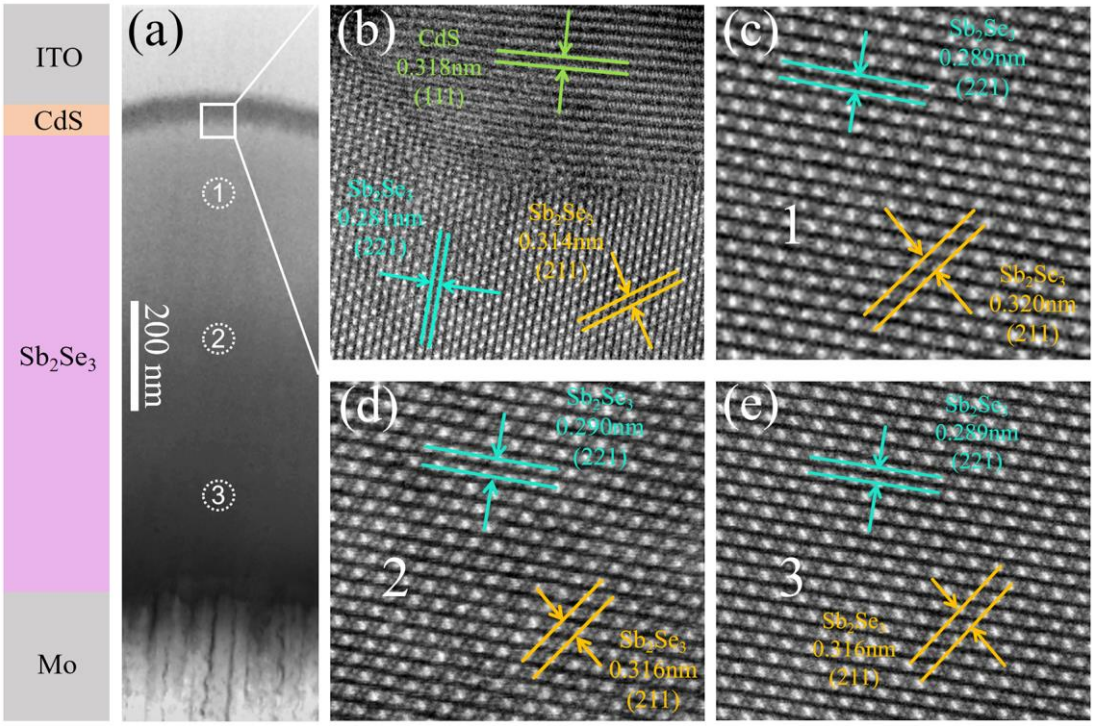

Fig. 7. Morphological and structural characterizations of the champion Sb_2Se_3 thin film solar cell. (a) Cross-sectional TEM image of the device, (b) HRTEM image of the Sb_2Se_3/CdS interface, (c-e) Lattice fringes correspond to three arbitrary spots 1, 2 and 3 across the Sb_2Se_3 absorber layer selected in (a) and performed by HRTEM.